





Pressure study on the interplay between magnetic order and valence crossover in $\text{EuPd}_2(\text{Si}_{1-x}\text{Ge}_x)_2$

Bernd Wolf , Theresa Lundbeck, Jan Zimmermann, Marius Peters, Kristin Kliemt , Cornelius Krellner , and Michael Lang
Physikalisches Institut, Goethe-Universität, 60438 Frankfurt (M), Germany

 (Received 15 March 2023; accepted 20 June 2023; published 30 June 2023)

We present results of the magnetic susceptibility on high-quality single crystals of $\text{EuPd}_2(\text{Si}_{1-x}\text{Ge}_x)_2$ for Ge concentrations $0 \leq x \leq 0.105$ performed under varying hydrostatic (He-gas) pressure $0 \leq p \leq 0.5$ GPa. The work extends recent studies at ambient pressure demonstrating the drastic change in the magnetic response from valence-crossover behavior for $x = 0$ and 0.058, to long-range antiferromagnetic (AFM) order below $T_N = 47$ K for $x = 0.105$. The valence-crossover temperature T_V' shows an extraordinarily strong pressure dependence of $dT_V'/dp = +(80 \pm 10)$ K/GPa. In contrast, a very small pressure dependence of $dT_N/dp \leq +(1 \pm 0.5)$ K/GPa is found for the AFM order upon pressurizing the $x = 0.105$ crystal from $p = 0$ to 0.05 GPa. Remarkably, by further increasing the pressure to 0.1 GPa, a drastic change in the ground state from AFM order to valence-crossover behavior is observed. Estimates of the electronic entropy related to the Eu $4f$ electrons, derived from analyzing susceptibility data at varying pressures, indicate that the boundary between AFM order and valence crossover represents a first-order phase transition. Our results suggest a particular type of second-order critical end point of the first-order transition for $x = 0.105$ at $p_{\text{cr}} \approx 0.06$ GPa and $T_{\text{cr}} \approx 39$ K where intriguing strong-coupling effects between fluctuating charge, spin, and lattice degrees of freedom can be expected.

DOI: [10.1103/PhysRevB.107.245147](https://doi.org/10.1103/PhysRevB.107.245147)

I. INTRODUCTION**A. Valence transition and critical end point**

In the vicinity of a second-order critical end point (CEP) which terminates a first-order phase transition line, strong fluctuations are expected which provide deep insight into the system's universal properties. Of particular interest are materials with correlated electrons tuned to a CEP by the application of pressure. For these systems strong-coupling effects between the correlated electrons and the lattice degrees of freedom can be expected [1]. As an example we mention the phenomenon of *critical elasticity* recently observed upon pressure-tuning an organic Mott insulator close to the CEP of the first-order Mott transition line [2]. A pronounced softening of the lattice was observed over a considerably wide T - p range around the CEP, indicating a particular strong coupling between the critical electronic system and the lattice degrees of freedom.

Similar strong-coupling effects can be expected also for other CEPs amenable to pressure tuning. In this regard, the valence-transition CEP represents a particularly interesting scenario as this transition involves, besides the charge and lattice degrees of freedom, also significant changes in the system's magnetic properties. Rare-earth-based intermetallics have been intensively used as target materials for studying valence fluctuations and their interplay with magnetism [3–13]. Based on these investigations a temperature-pressure (T - p) phase diagram for several Eu-based compounds has been derived [14–18]. At low pressures, the Eu ions are in their large-volume Eu^{2+} states which carry a local magnetic moment. The coupling between these moments, mediated via the Ruderman-Kittel-Kasuya-Yoshida (RKKY) interaction, usually gives rise to long-range antiferromagnetic (AFM) order at $T \leq T_N$. By the application of pressure the system adopts

a nonmagnetic low-volume $\text{Eu}^{(3-\delta)+}$ ($0 < \delta < 1$) state by crossing a first-order valence-transition line $T_V(p)$ (for $T > T_N$) [14,19]. This first-order line $T_V(p)$ terminates at a second-order CEP. On the high-pressure side of the CEP crossover behavior is expected and experimentally observed [14,16,18].

B. The case of EuPd_2Si_2

There are a few cases where a valence change can be induced by varying the temperature at ambient pressure [19–21]. Among them is EuPd_2Si_2 [22], which crystallizes in the tetragonal ThCr_2Si_2 structure. Upon cooling, the system shows a pronounced but still continuous valence change from $\text{Eu}^{2.3+}$ at high temperatures (around 300 K) to $\text{Eu}^{2.8+}$ below about 100 K [20,22,23]. This valence crossover manifests itself in a slightly broadened drop in the magnetic susceptibility within a narrow temperature interval of about 40 K [14,24–26]. A crossover temperature $T_V' \approx 160$ K has been assigned by using the position where the change in the magnetic susceptibility is largest [25,26]. The notion of a valence crossover in EuPd_2Si_2 is consistent with earlier findings on polycrystalline material [19,27], locating the system on the high-pressure side of the CEP. The research on this material has regained momentum recently thanks to the success in growing large single crystals of pure EuPd_2Si_2 [14,24] and Ge-substituted $\text{EuPd}_2(\text{Si}_{1-x}\text{Ge}_x)_2$ [25].

In the present work we focus on the effects of Ge substitution and hydrostatic pressure on the valence-crossover behavior, aiming at identifying suitable parameters by which the system can be tuned close to its CEP. Details on the single-crystal growth and sample characterization via magnetic susceptibility, thermal expansion, and structural investigations can be found in Refs. [24,25]; see also Ref. [26] for a preliminary account of magnetic susceptibility and thermal expansion

TABLE I. List of $\text{EuPd}_2(\text{Si}_{1-x}\text{Ge}_x)_2$ single crystals investigated. Given are the real Ge concentrations x_{real} determined by EDX analysis [25], the individual sample number, the valence-crossover temperature T'_V and its pressure dependence dT'_V/dp , as well as the Néel temperature T_N characterizing the transition into antiferromagnetic order.

x_{real}	Sample number	T'_V (K)	dT'_V/dp (K/GPa)	T_N (K)
		$p = 0$		$p = 0$
0	1	155 ± 1.5	80 ± 5	
0	2	120 ± 1.5	80 ± 5	
0.058(7)	3	90 ± 1.5	75 ± 5	
		$p = 0.1 \text{ GPa}$	$p \geq 0.1 \text{ GPa}$	$p = 0$
0.105(8)	4	45 ± 1.3	90 ± 10	47.3 ± 0.2
0.105(8)	5	45 ± 1.3	100 ± 10	47.3 ± 0.2

results as well as Ref. [28] for Raman-spectroscopy data. By employing susceptibility measurements in combination with fine (He-gas) pressure tuning under truly hydrostatic-pressure conditions, we find strong indications for the existence of a particular type of CEP, referred to as ‘‘CEP,’’ for single-crystalline $\text{EuPd}_2(\text{Si}_{1-x}\text{Ge}_x)_2$ with $x = 0.105$. We argue that, different from the valence-transition CEP implied in the generalized phase diagram [14–18], where the valence-crossover state emerges from a paramagnetic phase, the ‘‘CEP’’ for $x = 0.105$ marks the end point of a first-order transition line separating long-range AFM order from a valence-crossover state. Our results indicate that the ‘‘CEP’’ for the $x = 0.105$ compound is located at $p_{\text{cr}} \approx 0.06 \text{ GPa}$ and $T_{\text{cr}} \approx 39 \text{ K}$ making it readily accessible for future experiments aiming at a detailed investigation of the expected strong-coupling effects.

II. METHODS: EXPERIMENTS

Single crystals of $\text{EuPd}_2(\text{Si}_{1-x}\text{Ge}_x)_2$ with Ge concentrations $x = 0$ (crystals 1 and 2), 0.058 (crystal 3), and 0.105 (crystals 4 and 5) were grown by using the Czochralski method. Table I gives a list of the crystals investigated along with some characteristic temperatures and their pressure dependence as obtained in the present study. Details of the crystal growth, the determination of the real germanium concentration by energy-dispersive x-ray analysis (EDX), and results of some basic structural, magnetic, and thermodynamic investigations can be found in Refs. [24–26]. In what follows we refer to these crystals by their real Ge concentration and specify each individual sample by a sample number. The susceptibility was measured by using a commercial superconducting quantum interference device (SQUID) magnetometer (MPMS; Quantum Design) equipped with a CuBe pressure cell (Unipress Equipment Division, Institute of High Pressure Physics, Polish Academy of Science). The pressure cell is connected via a CuBe capillary to a room-temperature He-gas compressor, serving as a gas reservoir. This setup enables temperature sweeps over wide temperature ranges $2 \text{ K} \leq T \leq 300 \text{ K}$ to be performed at almost ideal $p = \text{constant}$ conditions, up to a maximum pressure of $p_{\text{max}} = 0.6 \text{ GPa}$; see Ref. [29] for details. For the interpretation of the

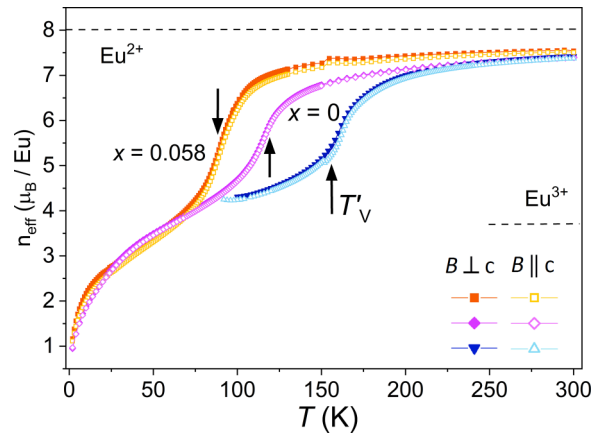


FIG. 1. Effective magnetic moment as a function of temperature for single crystals of $\text{EuPd}_2(\text{Si}_{1-x}\text{Ge}_x)_2$ with $x = 0$ [crystals 1 (blue symbols) and 2 (purple symbols)] and $x = 0.058$ (crystal 3). The data were taken in a magnetic field of 1 T for orientations parallel (open symbols) and perpendicular (closed symbols) to the tetragonal c axis. The dashed lines represent the full effective moment of free Eu^{2+} ($4f^7$) and Eu^{3+} ($4f^6$) ions at 300 K with a typical energy difference of $\sim 450 \text{ K}$ between the ground state and the first excited state [30]. Arrows indicate the valence-crossover temperature T'_V derived from the maximum position in $d(\chi T)/dT$. The small anomalies around 150 K are of extrinsic nature.

experimental results, it is important to note that for all pressure experiments reported here, helium is in its liquid state ensuring ideal hydrostatic-pressure conditions.

III. EXPERIMENTAL RESULTS

A. Overview of the magnetic behavior for crystals with $0 \leq x \leq 0.105$ at ambient pressure

In Figs. 1 and 2 we give an overview of the different magnetic behaviors revealed for single-crystalline $\text{EuPd}_2(\text{Si}_{1-x}\text{Ge}_x)_2$ in response to small changes in the Ge content from $x \leq 0.058$ (Fig. 1) to $x = 0.105$ (Fig. 2). To this end we plot the effective magnetic moment n_{eff} and its evolution with temperature for $2 \text{ K} \leq T \leq 300 \text{ K}$ as derived from magnetic susceptibility data $\chi(T)$ [25,26] via $n_{\text{eff}} = 2.828[\chi(T)T]^{1/2}$ in cgs units by using a spectroscopic g factor of 2. By plotting the data in this representation, small T -induced changes in the magnetic moment at high temperatures can be easily discerned. The measurements were carried out at ambient pressure, labeled $p = 0$ from here on, by applying a magnetic field of $B = 1 \text{ T}$ both parallel (open symbols) and perpendicular (closed symbols) to the tetragonal c axis. Figure 1 shows $n_{\text{eff}}(T)$ of two nonsubstituted single crystals $x = 0$ (crystals 1 and 2) and of a crystal with $x = 0.058$ (crystal 3). The data for $x = 0$ show a gradual reduction of n_{eff} on cooling from 300 K, followed by a more rapid drop within a rather narrow temperature window around 155 K (120 K) for crystal 1 (2). The significant reduction in n_{eff} to a value close to that of Eu^{3+} is assigned to the temperature-induced valence crossover from $\text{Eu}^{(2+\delta)+}$ to $\text{Eu}^{(3-\delta'+)+}$ [25,26], consistent with earlier results on polycrystalline material for $x = 0$ [27,31]. To parametrize this crossover behavior, we use the quantity $d(\chi T)/dT$ (cf. inset of Fig. 3 and Fig. 11 in

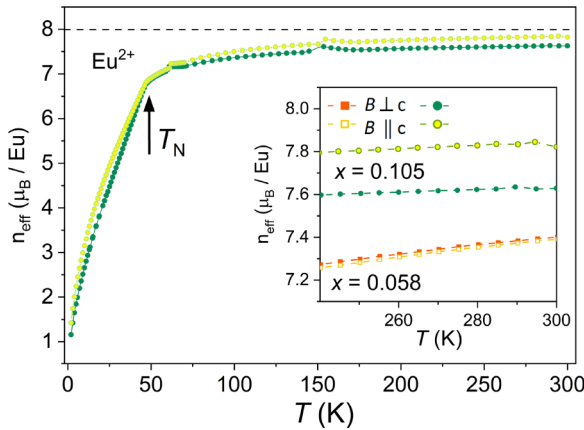


FIG. 2. Effective magnetic moment n_{eff} as a function of temperature for a single crystal of $\text{EuPd}_2(\text{Si}_{1-x}\text{Ge}_x)_2$ with $x = 0.105$ (crystal 5). The data were taken in a magnetic field of 1 T for orientations parallel (open symbols) and perpendicular (closed symbols) to the tetragonal c axis. The dashed horizontal line represents the full effective moment of free Eu^{2+} ($4f^7$) ions. The small anomalies around 150 K and 75 K are of extrinsic nature. The inset shows a blowup of the data for $T > 240$ K for highlighting the magnetic anisotropy. For comparison the inset also includes the data for the crystal with $x = 0.058$ (crystal 3) (cf. Fig. 1) in the same temperature range.

Appendix C for details), yielding Lorentzian-shaped curves within the crossover regime. We refer to the maximum in $d(\chi T)/dT$ as the valence-crossover temperature T'_V ; see Table I for a compilation of the so-derived T'_V values. Further characteristics of the data for the $x = 0$ crystals in Fig. 1 include a significant variation of T'_V for the two $x = 0$ crystals 1 and 2 investigated, and an almost isotropic magnetic behavior throughout the entire temperature range investigated; see also inset of Fig. 2. For the Ge-substituted crystal with $x = 0.058$ (crystal 3), we observe a similar behavior in $n_{\text{eff}}(T)$ albeit with a significant reduction of T'_V down to 90 K accompanied by an enhanced drop in n_{eff} down to about the same value as observed for $x = 0$. The data for $x \leq 0.058$ shown in Fig. 1 all share the same weak magnetic anisotropy, i.e., an $n_{\text{eff}}(B \perp c)$ which only slightly exceeds $n_{\text{eff}}(B \parallel c)$ throughout the entire temperature range investigated.

In Fig. 2 we show $n_{\text{eff}}(T)$ for $2 \text{ K} \leq T \leq 300 \text{ K}$ for a single crystal with $x = 0.105$ (crystal 5). Almost identical data (not shown) were obtained for a second crystal (crystal 4) of the same substitution level with only small differences for temperatures below 20 K. The data reveal a distinctly different behavior from that observed for $x \leq 0.058$ in Fig. 1, in showing a sharp kink at around 47 K which separates a slowly varying and somewhat enhanced n_{eff} at high temperatures from a rapidly decreasing n_{eff} down to lowest temperatures. We assign this behavior to long-range AFM order below $T_N = 47.3 \text{ K}$; see Refs. [25,26] for detailed investigations in support of this claim, including magnetic, thermodynamic, and structural investigations. In particular the study in Ref. [25] revealed an easy-plane magnetic anisotropy below T_N which is typically observed in Eu-based magnets; see also Sec. IV C.

Another, more subtle difference in the magnetic behavior of the $x = 0.105$ crystal as opposed to that observed for

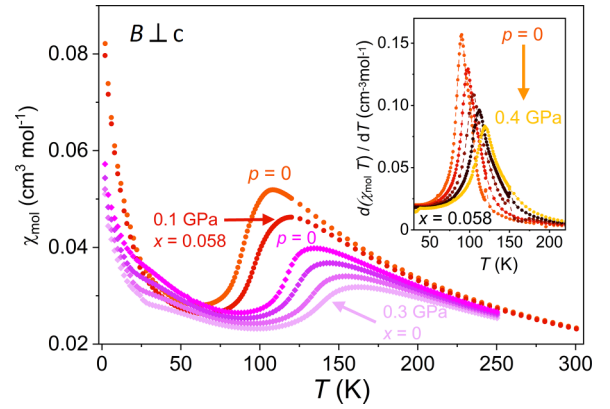


FIG. 3. Molar magnetic susceptibility as a function of temperature of single crystals of $\text{EuPd}_2(\text{Si}_{1-x}\text{Ge}_x)_2$ with $x = 0$ (crystal 2) and $x = 0.058$ (crystal 3) at varying pressures $p \leq 0.4$ GPa. The magnetic field of $B = 1$ T was oriented perpendicular to the tetragonal c axis. The inset exhibits the temperature derivative of χT of the crystal with $x = 0.058$ (crystal 3) for $0 \leq p \leq 0.4$ GPa in a narrow temperature window around T'_V .

lower Ge content relates to the magnetic anisotropy in the paramagnetic regime $T > T_N$. As shown in the inset of Fig. 2 we find that the anisotropy for the crystal with $x = 0.105$ is enhanced and reversed, now yielding an $n_{\text{eff}}(B \parallel c)$ which is significantly larger than $n_{\text{eff}}(B \perp c)$. This observation indicates changes in the local Eu^{2+} environment for the $x = 0.105$ samples, exhibiting AFM order, as opposed to the crystals showing valence-crossover behavior (see discussion Sec. IV B for more details).

B. Magnetic susceptibility at varying hydrostatic pressure

After having recapitulated the marked changes revealed in the magnetic response from valence-crossover behavior for $x \leq 0.058$ to long-range AFM order for $x = 0.105$, we will now focus on the effect of hydrostatic pressure on the respective behavior. To this end we show in Fig. 3 susceptibility data for B perpendicular to the c axis, χ_{\perp} , for crystals with $x = 0$ (crystal 2) and $x = 0.058$ (crystal 3) as a function of temperature at varying hydrostatic pressures $p \leq 0.4$ GPa. For both substitution levels we find pronounced changes in χ_{\perp} with pressure at intermediate temperatures, manifesting themselves in a significant shift of the valence-crossover temperature T'_V to higher temperatures, accompanied by a pronounced broadening of the crossover region. This is shown in more detail in the inset of Fig. 3, where the quantity $d(\chi T)/dT$ for crystal 3 ($x = 0.058$) is plotted for varying pressures $0 \leq p \leq 0.4$ GPa in a narrow temperature window around T'_V . By identifying the position of the maximum with T'_V , we find a pressure dependence of $dT'_V/dp = +(75 \pm 5) \text{ K/GPa}$; cf. Table I. These curves, which can be well described by a Lorentzian function (see Fig. 11 in Appendix C), also enable us to quantify the width of the valence-crossover region by using the full width at half maximum Γ of the Lorentzian. The crossover temperature T'_V as well as the width Γ will be used below (Figs. 6 and 7) for constructing the T - p phase diagram. Figure 3 demonstrates that there is a strong effect of pressure on χ_{\perp} for temperatures within the valence-crossover region.

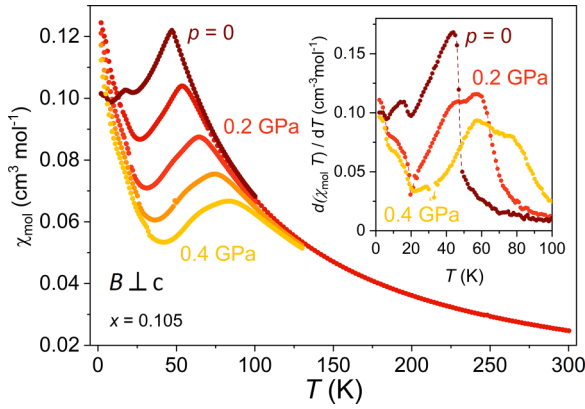


FIG. 4. Molar magnetic susceptibility as a function of temperature of a single crystal of $\text{EuPd}_2(\text{Si}_{1-x}\text{Ge}_x)_2$ with $x = 0.105$ (crystal 4) for varying pressure $0 \leq p \leq 0.4$ GPa. The external magnetic field of $B = 1$ T was oriented perpendicular to the tetragonal c axis. The inset shows the temperature derivative of (χT) of the data taken at $p = 0, 0.2$ GPa, and 0.4 GPa in a narrow temperature window using the same color code.

In contrast, there is only a minor effect that pressure has on χ_{\perp} outside this regime, i.e., for temperatures above about 220 K and below about 25 K. In particular, we mention the strong upturn in χ_{\perp} at low temperatures which is practically unaffected by the applied pressure. We consider this upturn as a characteristic feature of all crystals showing a valence crossover; see Sec. IV B below.

A qualitatively different behavior is visible in Fig. 4 where we show χ_{\perp} of a crystal with $x = 0.105$ (crystal 4) under varying pressure $p \leq 0.4$ GPa. The data at $p = 0$ reveal a sharp kink at $T_N = 47.3$ K followed by a rapid decrease down to lower temperatures. Apart from the small feature around 25 K and the mild upturn below about 10 K, the data are very similar to that obtained for crystal 5 (not shown) sharing the same Ge concentration of $x = 0.105$ within the resolution of the EDX analysis [25]. On increasing the pressure to $p = 0.1$ GPa and beyond, however, marked differences in the characteristics of χ_{\perp} become apparent. These include the onset of a pronounced upturn in χ_{\perp} at low temperatures, which is absent for $p = 0$, and a progressive rounding of the peak in χ_{\perp} with increasing pressure. The broadening becomes particularly clear for the data taken at 0.3 and 0.4 GPa, which bear all the characteristics of the valence crossover revealed for the crystals with $x = 0$ and 0.058 (Fig. 3), i.e., the slightly rounded pronounced drop in the susceptibility which lacks an easy-plane anisotropy, the strong pressure dependence of this feature, and a low-temperature upturn which is practically pressure independent. These observations suggest a pressure-induced change in the ground state for the $x = 0.105$ crystal from AFM order at $p = 0$ to a valence-crossover behavior at $p \geq 0.1$ GPa.

This notion is further corroborated by evaluating the quantity $d(\chi T)/dT$ and its variation with pressure shown in the inset of Fig. 4. For $p = 0$ a single strongly asymmetric peak is observed. As argued in Appendix B, where we compare $d(\chi T)/dT$ with the contribution to the specific heat related to the $4f$ electrons, this magnetic response is consistent

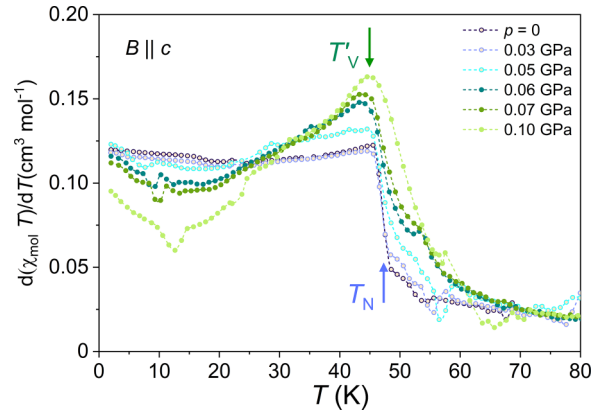


FIG. 5. Temperature derivative $d(\chi_{\parallel} T)/dT$ of single-crystalline $\text{EuPd}_2(\text{Si}_{1-x}\text{Ge}_x)_2$ with $x = 0.105$ (crystal 4) for varying small pressures $0 \leq p \leq 0.1$ GPa. The external field of $B = 1$ T was oriented along the tetragonal c axis. The position of the magnetic phase transition at T_N is marked by a blue up arrow, whereas the valence-crossover temperature T'_V is indicated by a green down arrow.

with a mean-field-type magnetic phase transition. In contrast, more symmetric though increasingly broadened behavior is revealed in $d(\chi T)/dT$ at higher pressures $p \geq 0.1$ GPa. As demonstrated for $x = 0.058$ in the inset of Fig. 3, a symmetric Lorentzian-like behavior in $d(\chi T)/dT$ characterizes the valence crossover. As will be discussed below, we attribute the broadening of these symmetric curves for $x = 0.105$ to sample inhomogeneities, i.e., small variations in the actual Ge concentration, resulting in a convolution of Lorentzian curves, each of which having a slightly different pressure dependence. To account for this broadening, both the low- and high-temperature flanks were fitted by Lorentzian curves and the pressure-induced shifts of each of which were determined. By using the average value we find $T'_V = (45 \pm 1.3)$ K at $p = 0.1$ GPa and $dT'_V/dp = +(90 \pm 10)$ K/GPa for crystal 4. Practically identical behavior, i.e., a mean-field-type phase transition anomaly in $d(\chi T)/dT$ that develops into broadened Lorentzian-type curves under pressure, was found for the second crystal (crystal 5) with $x = 0.105$ in measurements performed at $p = 0, 0.1, 0.2,$ and 0.4 GPa; see Table I for the characteristic temperatures and their pressure dependence.

The data in Fig. 4 suggest that hydrostatic pressure as small as $p = 0.1$ GPa is sufficient to induce a drastic change in the ground state for crystals with $x = 0.105$. To explore this interesting part of the T - p phase diagram in more detail, we show in Fig. 5 a series of χ_{\parallel} data plotted as $d(\chi T)/dT$ for temperatures $T \leq 80$ K at varying pressure $p \leq 0.1$ GPa. By using χ_{\parallel} as a probe for this investigation, we take advantage of the anisotropy that characterizes the AFM order at $p = 0$. As shown in Ref. [25], χ_{\parallel} is almost T independent in the magnetically-ordered state, reflecting an easy-plane anisotropy below T_N , whereas it shows a rapid drop in the valence-crossover regime. As a result, χ_{\parallel} is more sensitive than χ_{\perp} for probing a pressure-induced change from magnetic order to valence crossover.

The data in Fig. 5 reveal practically identical behavior in $d(\chi_{\parallel} T)/dT$ for $p = 0$ and 0.03 GPa, yielding an almost

T -independent behavior for $T \leq T_N = 47.3$ K and a sharp steplike change at T_N (up arrow in Fig. 5). This behavior reflects a mean-field-type phase transition into AFM order (see Appendix B). As there is no identifiable shift in T_N within the experimental resolution on increasing pressure from $p = 0$ to 0.03 GPa, we estimate an upper bound for the pressure dependence for the magnetic ordering temperature of $dT_N/dp \leq +(1 \pm 0.5)$ K/GPa. This small upper limit of the pressure dependence characterizing T_N is also consistent with the data at $p = 0.05$ GPa, which essentially show the same behavior as for $p \leq 0.03$ GPa at the steplike change, with some small deviations becoming visible on its low- and high-temperature side. By a mild increase of the pressure to 0.06 GPa, however, the shape of the anomaly in $d(\chi_{\parallel}T)/dT$ changes noticeably in developing a rounded peak and by progressively adopting a more symmetric Lorentzian-like shape. By identifying the position of the maximum with the valence-crossover temperature T'_V (down arrow in Fig. 5), the data in Fig. 5 yield a pressure dependence of $dT'_V/dp = +(50 \pm 20)$ K/GPa, which is of the same magnitude as the dT'_V/dp values revealed for the $x = 0$ and 0.058 compounds; cf. Table I. This pressure-induced alteration in the character of the anomaly is accompanied by the appearance of the low-temperature upturn in the susceptibilities χ_{\perp} (see Fig. 4) and χ_{\parallel} (not shown).

C. T - p phase diagrams

The anomalies associated with T'_V revealed in Figs. 3 and 4 are compiled in a T - p phase diagram (Fig. 6) of $\text{EuPd}_2(\text{Si}_{1-x}\text{Ge}_x)_2$ for $x = 0.058$ and $x = 0.105$. The diagram includes a range of negative pressure (gray area), not accessible by hydrostatic-pressure studies. For $x = 0.058$ the figure shows the valence-crossover temperature T'_V and its evolution with pressure for $p \leq 0.47$ GPa [32]. The figure also shows the width of the anomaly in $d(\chi T)/dT$, determined from the full width at half maximum value Γ of the Lorentzian curves fitted to the $d(\chi T)/dT$ data. In the pressure range investigated the so-derived values for T'_V as well as the lower and upper bounds of Γ all show to a good approximation a linear variation with pressure. This enables us to use a linear extrapolation to negative pressures (broken lines) in Fig. 6. For the $x = 0.058$ crystal, we find that these lines merge in a single point around $p_{\text{cr}} = -(0.63 \pm 0.05)$ GPa and $T_{\text{cr}} = (42 \pm 3)$ K. This point may serve as a good approximation for the location of the second-order CEP, shown as the gray filled circle in the main panel of Fig. 6. Applying a similar procedure to the $d(\chi T)/dT$ data for the $x = 0.105$ crystal (Fig. 4) for 0.06 GPa $\leq p \leq 0.4$ GPa results in a crossing point at $p_{\text{cr}} = -(0.15 \pm 0.05)$ GPa and $T_{\text{cr}} = (23 \pm 3)$ K. Note, that the crossover regime for the $x = 0.105$ crystal is delimited by the low- and high-temperature flanks of a convolution of Lorentz curves fitted to the broadened anomalies in $d(\chi T)/dT$ shown in the inset of Fig. 4. Despite the more complex behavior for the $x = 0.105$ compound, resulting from the appearance of magnetic order at low pressures, we may conclude from the trend revealed in Fig. 6 that by increasing the Ge concentration in $\text{EuPd}_2(\text{Si}_{1-x}\text{Ge}_x)_2$, the CEP of the valence transition is shifted to lower temperatures and is moved closer to $p = 0$.

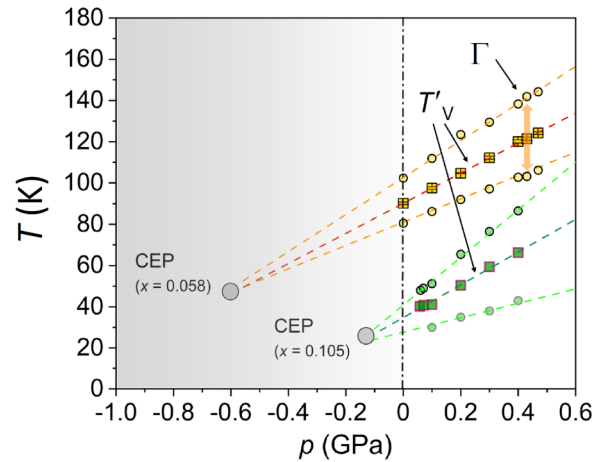


FIG. 6. T - p phase diagram of $\text{EuPd}_2(\text{Si}_{1-x}\text{Ge}_x)_2$ with $x = 0.058$ and $x = 0.105$ constructed by analyzing $d(\chi T)/dT$ data of crystals 3 and 4, respectively. The range of negative pressure is indicated in gray. The width of the crossover regime is visualized by pairs of filled circles, the distance of which (indicated by the double arrow) corresponds to the full width at half maximum value Γ of the Lorentzian curves fitted to the $d(\chi T)/dT$ data. The broken and dotted lines are used to extrapolate anomalies related to T'_V and to the width of the crossover line Γ to negative pressures. The point of intersection of these lines (large gray sphere) is considered as a good approximation for the location of the critical end point (CEP).

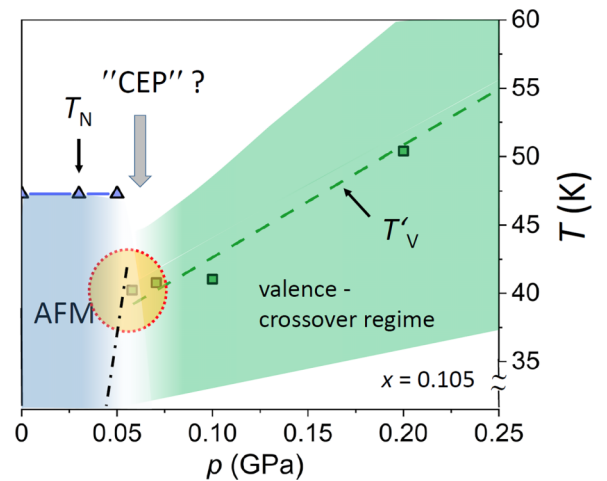


FIG. 7. Details of the T - p phase diagram of $\text{EuPd}_2(\text{Si}_{1-x}\text{Ge}_x)_2$ with $x = 0.105$ based on the analysis of $d(\chi T)/dT$ data of crystal 4. The figure shows the antiferromagnetic (AFM) phase (blue shaded area) below T_N , the valence-crossover regime (green shaded region) visualized by the crossover temperature T'_V , and the width of Lorentzian curves fitted to the $d(\chi T)/dT$ data. The black broken line separating the two phases serves as a guide to the eyes. As argued in the main text, this broken line is likely representing a first-order phase transition terminating in a second-order critical end point, referred to as “CEP” (red circle). According to the Clausius-Clapeyron equation, see Sec. IV D of the discussion, we expect a positive pressure dependence of the first-order phase transition line.

Figure 7 shows details of the T - p phase diagram for the $x = 0.105$ crystal (crystal 4) in a narrow pressure window $0 \leq p \leq 0.25$ GPa. The figure includes the region of long-range AFM order (blue shaded area) below T_N , which is practically pressure independent on the pressure scale shown here. At pressures of $p \geq 0.06$ GPa, where no indications for magnetic order can be revealed for $T \geq 2$ K, the material is in the valence-crossover region, visualized by the crossover line T'_V . In contrast to T_N , this crossover line T'_V reveals a strong pressure dependence. The data obtained for crystal 5 with the same $x = 0.105$ were found to be fully consistent with the results shown in the phase diagram in Fig. 7. The figure highlights the exceptional character of the $x = 0.105$ crystal in showing an extraordinarily high sensitivity of its ground state to hydrostatic pressure.

IV. DISCUSSION

A. Effects of physical pressure, Ge substitution, and disorder on the valence crossover

The present investigations on single-crystalline $\text{EuPd}_2(\text{Si}_{1-x}\text{Ge}_x)_2$ with $x = 0, 0.058, \text{ and } 0.105$ highlight the strong sensitivity of the valence-crossover behavior to various parameters. These include the Ge concentration x , the effect of hydrostatic pressure, as well as the influence of disorder. The latter effect manifests itself particularly clearly in the marked sample-to-sample variations revealed for crystals 1 and 2 with $x = 0$ (cf. Fig. 1). Before discussing the effects of pressure and Ge substitution, we start by addressing the influence of disorder.

As shown in Ref. [24] for the $x = 0$ crystals, there are small variations in the Pd:Si ratio along the growth direction of the crystals with the Pd site (Wyckoff position $4d$) being partially occupied by up to 3% Si while for all samples the $4e$ Wyckoff position is completely occupied with Si. As a result of this site-exchange-type of disorder in the Pd-Si layers, there are small changes in the regular Si positions, and correspondingly, the bond lengths [24]. The influence of these changes, especially the a -axis lattice parameter on T'_V , has also been revealed by DFT calculations [33]. Since for the $x = 0$ crystals all lattice parameters are found to be modified by the Pd:Si ratio [25], with the structural changes being at the limit of the experimental resolution in XRD, it is difficult to correlate changes in T'_V to changes of the lattice parameters.

This is different for the Ge-substituted crystals where a clear correlation between an increase of the a -axis lattice parameter and a decrease in T'_V can be observed upon increasing x [25]. Our observations seem to indicate that sample-to-sample variations are much less pronounced; cf. the practically identical magnetic behavior revealed for crystals 4 and 5 with $x = 0.105$. In particular, we find identical behavior for these crystals in the valence-fluctuating regime at $p \geq 0.1$ GPa. In these substituted crystals, the Ge atoms because of their size, being significantly larger than Si but similar to Pd, are expected to preferably participate in the site exchange on the Pd position. As a result these Pd-Ge site-exchange processes will only weakly influence the regular Si positions in the surrounding. This favorable side effect of weak Ge

substitution may provide a rationale for the lack of significant sample-to-sample variations in T'_V revealed in this study for the crystals with $x > 0$.

As for the effect of pressure, the application of He-gas pressure to single crystals at various substitution levels has demonstrated a strong pressure dependence of T'_V with rates dT'_V/dp ranging from $+(100 \pm 10)$ K/GPa ($x = 0.105$) to about $+(75 \pm 5)$ K/GPa ($x = 0.058$). The strong increase of T'_V with pressure is accompanied by a significant widening of the valence-crossover range. An extraordinarily high pressure dependence of the valence transition as well as the width of the valence-crossover region are typical characteristics for valence-fluctuating Eu compounds [16,34]. In the pressure range investigated we find that both T'_V and also the width Γ vary linearly with pressure. By using a linear extrapolation to negative pressures these lines merge in a single point. We consider this point as a good approximation for the location of the (hypothetical) second-order CEP out of which crossover regimes are expected to emanate in a V-shaped manner; see, e.g., Ref. [2]. The data for $x = 0.058$ and 0.105 , which are likely to be less affected by disorder effects as suggested above, indicate that increasing the Ge concentration x corresponds to a shift of the critical pressure by $\Delta p > 0$. This notion is consistent with the results on polycrystalline samples with $x = 0$, yielding a critical pressure above 0.7 GPa [19,35]. It is tempting to attribute this effect to the negative chemical pressure induced by replacing the smaller Si atoms by the larger (isoelectronic) Ge atoms, corresponding to a widening of the lattice; see also Ref. [25].

B. Low-temperature increase in susceptibility for $x = 0$ and 0.058

The results of the magnetic susceptibility shown in Figs. 3 and 4 demonstrate that there is a strong increase in $\chi(T)$ at low temperatures $T \leq 25$ K for the crystals showing valence-crossover behavior. In contrast to the crossover temperature T'_V , which is strongly pressure dependent, this low-temperature upturn is practically unaffected by pressure. Furthermore, no effect is found upon increasing the field from 1 T to 5 T (not shown). These observations together with the fact that this upturn is very similar for all crystals investigated makes an interpretation in terms of an impurity contribution very unlikely. Rather it points to an origin which is intrinsic to the state below T'_V . This interpretation is consistent with experimental results obtained on various valence-fluctuating Ce and Yb compounds discussed in Ref. [3] and the references cited therein.

C. Antiferromagnetic order for $x = 0.105$

As discussed in detail in Ref. [25], the magnetic signatures revealed for $x = 0.105$ at $p = 0$, including a sharp kink at 47.3 K followed upon cooling by an easy-plane anisotropy, and a mean-field-type phase transition in the specific heat, provide clear evidence for long-range AFM order. This easy-plane anisotropy is also visible in the quantity $d(\chi T)/dT$ as displayed in Figs. 5 and 9. The observed T_N and its small pressure dependence revealed in the present work fall into the ranges typically observed for intermetallic compounds featur-

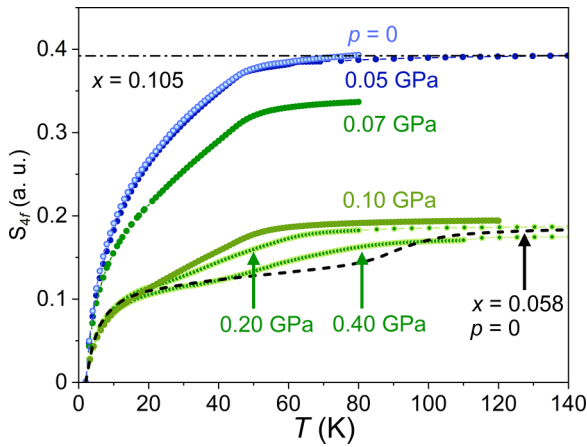


FIG. 8. Estimate of the entropy, S_{4f} , related to the $4f$ electrons of crystal 4 with $x = 0.105$ in arbitrary units obtained by integrating $[(1/T)d(\chi T)/dT] \propto C_{4f}/T$. See Appendix B for details. The light blue (full blue) circles represent S_{4f} at $p = 0$ (0.05 GPa), where the system adopts an antiferromagnetically ordered ground state. The dash-dotted line marks the maximum entropy S_{\max} , which is expected to be a sizable fraction of $R \ln(2S + 1)$ of the $S = 7/2$ state. The dark green circles correspond to S_{4f} at $p = 0.07$ GPa. The data obtained for $p = 0.1, 0.2,$ and 0.4 GPa (full light green circles) show a significantly reduced S_{4f} approaching about $0.5 S_{\max}$. The black dashed line corresponds to S_{4f} of the $x = 0.058$ crystal (crystal 3) at $p = 0$ which shows valence-crossover behavior.

ing divalent Eu ions; see Refs. [5,7–13,16,36] and references cited therein. In this context we also mention the magnetic anisotropy revealed in the paramagnetic state for $x = 0.105$ (see inset of Fig. 2), which is often seen in Eu^{2+} -based magnets, especially in the 122 compounds [36].

D. Pressure-induced change from antiferromagnetic order to valence-crossover behavior for $x = 0.105$

The T - p phase diagram in Fig. 7 for $x = 0.105$ indicates a drastic change in the material’s ground state from AFM order to valence crossover in response to a tiny increase in the applied pressure from 0.03 GPa to 0.06 GPa. The interplay between AFM order and valence fluctuations was discussed in a theoretical work by Watanabe and Miyake [37]. It was found that for strong valence fluctuations, the valence-crossover regime is separated from the magnetic state by a first-order phase transition. To explore the possibility of such a p -induced first-order transition in $\text{EuPd}_2(\text{Si}_{1-x}\text{Ge}_x)_2$ for $x = 0.105$ in more detail, we attempted to gain access to the entropy contribution of the $4f$ electrons, S_{4f} , for the $x = 0.105$ compound and to explore the variation of S_{4f} with pressure. To this end we again take advantage of the proportionality between $d(\chi T)/dT$ and the $4f$ -related electronic specific heat (see Fig. 10 in Appendix B for details). By using the experimental data shown in Figs. 3, 4, 5, and 9 and by integrating the expression $[(1/T)d(\chi T)/dT] \propto C_{4f}/T$, we get an estimate of the entropy related to the $4f$ electrons. An estimate of the $C_{4f}(T)$ contribution was obtained in Ref. [25] (see also Appendix B for details).

The so-derived $S_{4f}(T)$ is shown in Fig. 8 for varying pressure $p \leq 0.4$ GPa. The figure indicates that at $p = 0$, where

the system orders antiferromagnetically below $T_N = 47.3$ K, S_{4f} tends to level off at its highest value S_{\max} . Practically identical behavior within the experimental resolution is obtained for $p = 0.05$ GPa. On mildly increasing the pressure to 0.07 GPa, however, a significant reduction in the maximum entropy to $0.87 S_{\max}$ is observed. For pressures of 0.1, 0.2, and 0.4 GPa, where the system undergoes the valence crossover, the maximum entropy is further reduced to about $0.5 S_{\max}$. The data in Fig. 8 suggest that crossing the boundary between AFM order and valence crossover on increasing the pressure at $T = \text{constant}$ from 0.05 over 0.07 to 0.1 GPa is accompanied by a discontinuous change in entropy, indicative of a first-order phase transition. Moreover, according to the Clausius-Clapeyron equation $dT^*/dp = \Delta V/\Delta S$, a negative volume change $\Delta V < 0$, together with the drop in entropy $\Delta S < 0$ on going from the antiferromagnetically ordered state to the valence-crossover regime, corresponds to a positive pressure dependence of the corresponding first-order phase transition line T^* . In order to verify the first-order character of the transition, continuous pressure sweeps at $T = \text{constant}$ conditions of a thermodynamic probe would be desirable. Whereas pressure sweeps in combination with measurements of the specific heat or magnetization are very challenging, they are feasible for measurements probing the relative length changes [38,39]. As was demonstrated in Refs. [2,26] these experiments are very sensitive to the character of the phase transition and the presence of valence fluctuations and are thus considered key experiments for exploring this part of the phase diagram in detail.

An exciting implication of such a first-order phase transition would be the presence of a particular type of critical end point, referred to as “CEP,” where the valence crossover emerges directly out of an antiferromagnetically ordered state. In contrast to the CEP for canonical valence-fluctuating systems, where effects of interacting charge and lattice degrees of freedom are expected, here an additional degree of freedom resulting from the nearby magnetic order comes into play. As a result we may expect strong-coupling effects between spin, charge, and lattice degrees of freedom upon approaching this “CEP.” According to the phase diagram depicted in Fig. 7, we locate the critical end point for $x = 0.105$ at $p_{\text{cr}} \approx 0.06$ GPa and $T_{\text{cr}} \approx 39$ K.

V. CONCLUSIONS

The interplay between valence crossover ($x \leq 0.058$) and magnetic order ($x = 0.105$) has been investigated by measurements of the magnetic susceptibility on single-crystalline $\text{EuPd}_2(\text{Si}_{1-x}\text{Ge}_x)_2$ under varying hydrostatic (He-gas) pressure $p \leq 0.5$ GPa. At ambient pressure, the crystals with $x = 0$ and 0.058 show valence-crossover behavior with a crossover temperature T'_V ranging from 90 K to about 155 K. T'_V is characterized by a strong pressure dependence of typically $dT'_V/dp = +(80 \pm 10)$ K/GPa. On the other hand, for $x = 0.105$, as a consequence of negative chemical pressure, long-range AFM order is observed below $T_N = 47.3$ K. In contrast to the strong pressure dependence of T'_V , T_N remains practically unaffected by pressure for $p \leq 0.05$ GPa. On further increasing the pressure to 0.07 and 0.1 GPa, however, the $x = 0.105$ crystal changes its ground state from AFM order

to valence crossover. Estimates of the entropy contribution related to the $4f$ electrons indicate this transition to be of first order. Our results suggest the existence of a special second-order critical end point for $x = 0.105$ at $p_{cr} \approx 0.06$ GPa and $T_{cr} \approx 39$ K. Unlike the critical end point that terminates a first-order valence-transition line T_V , this end point distinguishes itself by valence-crossover behavior emerging directly out of an antiferromagnetically ordered state. As a result, strong-coupling effects between fluctuating charge, spin, and lattice degrees of freedom can be expected. The low value of p_{cr} , conveniently accessible by He-gas-pressure experiments, makes this system a well-suited target material for detailed investigations of such strong-coupling effects.

ACKNOWLEDGMENTS

We thank Ch. Geibel for fruitful discussions. This work was supported by the Deutsche Forschungsgemeinschaft (DFG; German Research Foundation) through TRR 288 (422213477, projects A01 and A03).

APPENDIX A: MAGNETIC ANISOTROPY

In order to estimate the electronic entropy S_{4f} from $d(\chi T)/dT$ data (see Appendix B), the anisotropy in the magnetic response has to be taken into account. Figure 9 shows the temperature derivative $d(\chi_{\perp} T)/dT$ for $x = 0.105$ (crystal 4) for varying small pressures $0 \leq p \leq 0.1$ GPa. In contrast to the corresponding plot for χ_{\parallel} (Fig. 5), the distinction between anomalies associated to T_N and T'_V are less clear for χ_{\perp} . The reason for that lies in the magnetic easy-plane anisotropy that develops below T_N , see Ref. [25] for χ_{\perp} and χ_{\parallel} data, manifesting itself in a rapidly decreasing χ_{\perp} as opposed to a practically T -independent χ_{\parallel} . A decreasing χ_{\perp} that is also revealed upon cooling through T'_V makes it more difficult to discriminate between both scenarios. Despite these difficulties, a clear statement can be made by analyzing the data on the high-temperature flank of the anomaly. For

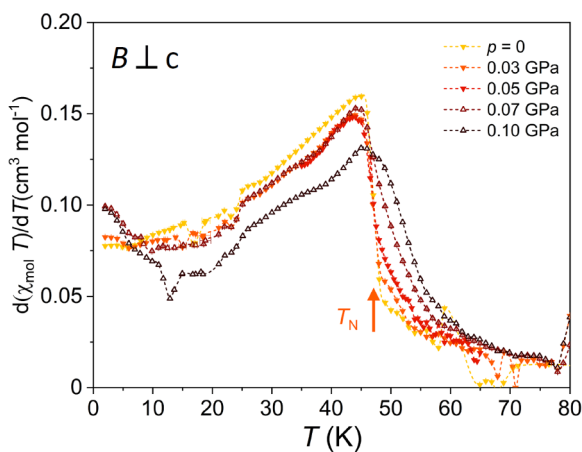


FIG. 9. Temperature derivative $d(\chi_{\perp} T)/dT$ of single-crystalline $\text{EuPd}_2(\text{Si}_{1-x}\text{Ge}_x)_2$ for $x = 0.105$ (crystal 4) at varying small pressures $0 \leq p \leq 0.1$ GPa. The external field of $B = 1$ T was oriented perpendicular to the c axis. The position of the magnetic phase transition at T_N is marked by a red up arrow.

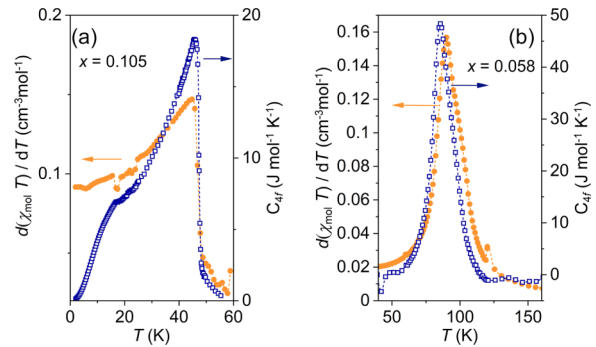


FIG. 10. Comparison of the $4f$ -related specific heat (right scales, open blue squares) of $\text{EuPd}_2(\text{Si}_{1-x}\text{Ge}_x)_2$ [25], with $d(\chi T)/dT$ (left scales, closed orange circles), plotted on the same temperature axes, for $x = 0.105$ (a) and 0.058 (b).

$0 \leq p \leq 0.05$ GPa the $d(\chi_{\perp} T)/dT$ data exhibit a steplike change, reminiscent of the mean-field-like phase transition anomaly observed in the specific heat at T_N (Fig. 10) without any resolvable pressure dependence. On further increasing the pressure to 0.07 and 0.1 GPa, however, a shoulder develops in $d(\chi_{\perp} T)/dT$ above 45 K, indicating a significant pressure dependence of this contribution. The data are consistent with a pressure-induced change from AFM order for $p \leq 0.05$ GPa to valence-crossover behavior for $p \geq 0.07$ GPa – the same conclusion as drawn by analyzing corresponding χ_{\parallel} data in Fig. 5.

APPENDIX B: ESTIMATE OF $4f$ ENTROPY

By using thermodynamic arguments Fisher showed that for antiferromagnets the quantity $d(\chi T)/dT$ is proportional to the magnetic specific heat [40]. Below we demonstrate that for the present $\text{EuPd}_2(\text{Si}_{1-x}\text{Ge}_x)_2$ system the proportionality between electronic contributions to the specific heat and $d(\chi T)/dT$ holds true not only for magnetic contributions around T_N but also for the contributions resulting from valence fluctuations around T'_V .

To this end we plot the $4f$ contribution to the specific heat, C_{4f} , for crystals with $x = 0.105$ [Fig. 10(a)] and 0.058 [Fig. 10(b)] (right scales) along with the corresponding $d(\chi T)/dT$ data (left scales). C_{4f} was obtained from the measured specific heat by subtracting the lattice contributions and a small non- $4f$ -related electronic contribution as described in detail in Ref. [25]. The lattice contribution was obtained by a Debye fit using two Debye temperatures [25]. To account for the non- $4f$ -related electronic contribution, i.e., the contributions of $\text{Eu } 5d$, $\text{Pd } 4d$, and $\text{Si } 3p$ states at the Fermi level, a term γT was used with $\gamma = 6$ mJ/mol K², found for the reference material LaPd_2Si_2 which lacks $4f$ electrons [25].

Figures 10(a) and 10(b) highlight the clear correspondence in the shape of the observed features, yielding asymmetric, mean-field-type phase transition anomalies in both quantities at the magnetic transition for $x = 0.105$ [Fig. 10(a)] as opposed to symmetric Lorentzian-shaped curves characterizing the valence crossover at T'_V [Fig. 10(b)]; see also Ref. [9] for corresponding $C(T)$ results on $\text{EuNi}_2(\text{Si}_{1-x}\text{Ge}_x)_2$. After having established this correspondence between $d(\chi T)/dT$ and the $4f$ -related electronic specific heat for these well-defined

borderline cases, we feel confident in using the quantity $d(\chi T)/dT$ also for identifying pressure-induced changes in the character of the anomalies for the crystal with $x = 0.105$ (cf. Fig. 4).

Besides the above qualitative statements, the correspondence between C_{4f} and $d(\chi T)/dT$ can be used also for estimating the $4f$ entropy S_{4f} . By integrating the expression $[(1/T)d(\chi T)/dT \propto C_{4f}/T]$ an estimate of the $4f$ entropy S_{4f} can be obtained. Note that in order to account for the magnetic anisotropy of the antiferromagnetically-ordered state, we use an expression $[d(\chi_{\perp} T)/dT + 2d(\chi_{\parallel} T)/dT]/3$ to estimate the magnetic entropy as a function of temperature at different pressures. By doing so we are able to follow the evolution of S_{4f} in small pressure steps. As displayed in Fig. 8, the so-derived $S_{4f} = S_{\text{mag}}$ for the crystal with $x = 0.105$, which orders antiferromagnetically below $T_N = 47.3$ K, shows the tendency to saturate at intermediate temperatures at a value S_{max} . A practically identical behavior is obtained on applying pressure of 0.05 GPa. On further increasing the pressure to 0.07 GPa, we observe a reduction to about $0.87 S_{\text{max}}$. Finally, for pressures of 0.1, 0.2, and 0.4 GPa, the highest pressure of our experiments, a plateau is reached at around 0.5 of S_{max} . About the same value is reached for the crystal with $x = 0.058$ at $p = 0$ (broken line) which shows valence-crossover behavior. The drastic change in S_{4f} on mildly increasing the pressure from 0.05 to 0.07 and finally 0.1 GPa is considered as a strong indication for a pressure-induced first-order transition on going from the antiferromagnetically-ordered state to the valence-crossover region.

APPENDIX C: MODELING OF $d(\chi T)/dT$

Figure 11 exhibits the temperature dependence of the quantity $d(\chi T)/dT$ at $p = 0$ and $p = 0.4$ GPa of $\text{EuPd}_2(\text{Si}_{1-x}\text{Ge}_x)_2$ with $x = 0.058$ for crystal 3. As discussed in the main text, these representations were used for parametrizing the valence-crossover regime and to construct the p - T phase diagram. The figure demonstrates that the

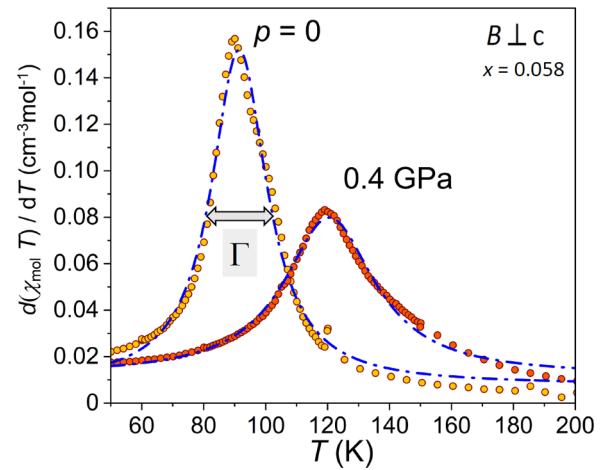


FIG. 11. Magnetic susceptibility data plotted as $d(\chi T)/dT$ of single-crystalline $\text{EuPd}_2(\text{Si}_{1-x}\text{Ge}_x)_2$ with $x = 0.058$ for crystal 3. The figure shows the data for $p = 0$ (full dark yellow circles) together with the data taken at $p = 0.4$ GPa (full red circles). The blue broken line is a fit to the data by using a Lorentzian function. The full width at half maximum Γ of the Lorentzian is indicated by the grey arrow.

Lorentzian curves (broken lines) provide a good fit to the data, capturing the characteristic features, namely the position of the maximum, the symmetric shape of the curves (around the maximum), as well as their width. For the latter, the full width at half maximum Γ (double arrow in Fig. 11) of the Lorentzian is used. The characteristic energy scale of the valence transition or valence crossover, characterized by the position of the maximum of the Lorentzian, corresponds to the energy difference between the $\text{Eu}^{2+}(4f^7)$ and $\text{Eu}^{3+}(4f^6)$ configurations. The corresponding interchange process between these two electronic configurations involves hopping of the localized $4f$ electrons to conduction band states and vice versa [41]. This process bears some resemblance of a damped oscillator, described by a Lorentzian function.

- [1] M. Zacharias, I. Paul, and M. Garst, Quantum Critical Elasticity, *Phys. Rev. Lett.* **115**, 025703 (2015).
- [2] E. Gati, M. Garst, R. S. Manna, U. Tutsch, B. Wolf, L. Bartosch, H. Schubert, T. Sasaki, J. A. Schlueter, and M. Lang, Breakdown of Hooke's law of elasticity at the Mott critical endpoint in an organic conductor, *Sci. Adv.* **2**, e1601646 (2016).
- [3] J. M. Lawrence, P. S. Riseborough, and R. D. Parks, Valence fluctuation phenomena, *Rep. Prog. Phys.* **44**, 1 (1981).
- [4] D. H. Ryan, S. L. Bud'ko, B. Kuthanazhi, and P. C. Canfield, Valence and magnetism in EuPd_3S_4 and $(\text{Y, La})_x\text{Eu}_{1-x}\text{Pd}_3\text{S}_4$, *Phys. Rev. B* **107**, 014402 (2023).
- [5] Z. Hossain, T. Strassel, C. Geibel, and A. Furrer, First-order valence transition and barocaloric effect in $\text{EuNi}_2(\text{Si}_{1-x}\text{Ge}_x)_2$, *J. Magn. Magn. Mater.* **272-276**, 2352 (2004).
- [6] M. A. Ahmida, M. K. Forthaus, C. Geibel, Z. Hossain, G. R. Hearne, J. Kastil, J. Prchal, V. Sechovsky, and M. M. Abd-Elmeguid, Charge fluctuations across the pressure-induced quantum phase transition in $\text{EuCu}_2(\text{Si}_{1-x}\text{Ge}_x)_2$, *Phys. Rev. B* **101**, 205127 (2020).
- [7] M. Baenitz, A. A. Gippius, A. K. Rajarajan, E. N. Morozova, Z. Hossain, C. Geibel, and F. Steglich, Crossover from divalent to valence fluctuating state of Eu in $\text{EuCu}_2(\text{Si}_{1-x}\text{Ge}_x)_2$ probed by $^{63,65}\text{Cu}$ -NMR, *Phys. B: Condens. Matter* **378-380**, 683 (2006).
- [8] M. Dionicio, H. Wilhelm, Z. Hossain, and C. Geibel, Temperature- and pressure-induced valence transition in EuCo_2Ge_2 , *Phys. B: Condens. Matter* **378-380**, 724 (2006).
- [9] Z. Hossain, C. Geibel, N. Senthilkumaran, M. Deppe, M. Baenitz, F. Schiller, and S. L. Molodtsov, Antiferromagnetism, valence fluctuation, and heavy-fermion behavior in $\text{EuCu}_2(\text{Si}_{1-x}\text{Ge}_x)_2$, *Phys. Rev. B* **69**, 014422 (2004).
- [10] S. E. Muthu, D. Braithwaite, B. Salce, A. Nakamura, M. Hedo, T. Nakama, and Y. Onuki, Calorimetry study of the phase diagram of EuNi_2Ge_2 , *J. Phys. Soc. Jpn.* **85**, 094603 (2016).
- [11] A. Nakamura, T. Okazaki, M. Nakashima, Y. Amako, K. Matsubayashi, Y. Uwatoko, S. Kayama, T. Kagayama, K. Shimizu, T. Uejo, H. Akamine, M. Hedo, T. Nakama, and Y. Onuki, Pressure-induced valence transition and heavy fermion

- state in EuNi_3Ge_5 and EuRhSi_3 , *J. Phys. Soc. Jpn.* **84**, 053701 (2015).
- [12] J. Gouchi, K. Miyake, W. Iha, M. Hedo, T. Nakama, Y. Onuki, and Y. Uwatoko, Quantum criticality of valence transition for the unique electronic state of antiferromagnetic compound EuCu_2Ge_2 , *J. Phys. Soc. Jpn.* **89**, 053703 (2020).
- [13] S. Fukuda, Y. Nakanuma, J. Sakurai, A. Mitsuda, Y. Isikawa, F. Ishikawa, T. Goto, and T. Yamamoto, Application of Doniach diagram on valence transition in $\text{EuCu}_2(\text{Si}_{1-x}\text{Ge}_x)_2$, *J. Phys. Soc. Jpn.* **72**, 3189 (2003).
- [14] Y. Ōnuki, F. Nakamura, T. Aoki, T. Tekeuchi, M. Nakahima, Y. Amako, K. Harima, K. Matsubayashi, Y. Uwatoko, S. Kayama, T. Kagayama, K. Shimizu, S. Esakki Muthu, D. Braithwaite, B. Salce, H. Shiba, T. Yara, Y. Ashitomi, K. Tomori, M. Hedo *et al.*, Divalent, trivalent and heavy fermion states in Eu compounds, *Philos. Mag.* **97**, 3399 (2017).
- [15] H. Wada, T. Sakata, A. Nakamura, A. Mitsuda, M. Shiga, Y. Ikeda, and Y. Bando, Thermal expansion and electric resistivity of $\text{EuNi}_2(\text{Si}_{1-x}\text{Ge}_x)_2$, *J. Phys. Soc. Jpn.* **68**, 950 (1999).
- [16] Y. Ōnuki, M. Hedo, and F. Honda, Unique electronic states of Eu-based compounds, *J. Phys. Soc. Jpn.* **89**, 102001 (2020).
- [17] B. K. Cho, J. S. Rhyee, and H. C. Ri, Antiferromagnetic order and valence fluctuation in $\text{EuPd}_2(\text{Ge}_{1-x}\text{Si}_x)_2$, *J. Phys. Soc. Jpn.* **71**, 252 (2002).
- [18] S. Seiro and C. Geibel, From stable divalent to valence fluctuating behaviour in $\text{Eu}(\text{Rh}_{1-x}\text{Ir}_x)_2\text{Si}_2$ single crystals, *J. Phys.: Condens. Matter* **23**, 375601 (2011).
- [19] B. Batlogg, A. Jayaraman, V. Murgai, L. C. Gupta, R. D. Parks, and M. Croft, Pressure-temperature studies and the p-T diagram of EuPd_2Si_2 , in *Valence Instabilities*, edited by P. Wachter and H. Boppert (Elsevier, Amsterdam, Netherlands, 1982), p. 229.
- [20] K. Mimura, S. M. A. Taguchi, Y. Fukuda, K. Sakurai, J. Ichikawa, and O. Aita, Bulk-sensitive high-resolution photoemission study of a temperature-induced valence transition system in EuPd_2Si_2 , *J. Electron Spectrosc. Relat. Phenom.* **137-140**, 529 (2004).
- [21] I. Felner and I. Nowik, First-order valence phase transition in cubic YbInCu_4 , *Phys. Rev. B* **33**, 617 (1986).
- [22] E. V. Sampathkumaran, K. Vijayaraghavan, V. Gopalakrishnan, R. Pillay, H. Devare, L. Gupta, B. Post, and R. Parks, Valence transition of EuPd_2Si_2 , in *Valence Fluctuations in Solids*, edited by M. L. Falicov, W. Hanke, and M. B. Maple (Elsevier, Amsterdam, Netherlands, 1981), p. 193.
- [23] M. Croft, J. A. Hodges, E. Kemly, A. Krishnan, V. Murgai, and L. C. Gupta, Cooperative Configuration Change in EuPd_2Si_2 , *Phys. Rev. Lett.* **48**, 826 (1982).
- [24] K. Kliemt, M. Peters, I. Reiser, M. Ocker, F. Walther, D.-M. Tran, E. Cho, M. Merz, A. Haghighirad, D. Hezel, F. Ritter, and C. Krellner, Strong influence of the Pd-Si ratio on the valence transition in EuPd_2Si_2 single crystals, *Cryst. Growth Des.* **22**, 5399 (2022).
- [25] M. Peters, K. Kliemt, M. Ocker, B. Wolf, P. Puphal, M. Le Tacon, M. Merz, M. Lang, and C. Krellner, From valence fluctuations to long-range magnetic order in $\text{EuPd}_2(\text{Si}_{1-x}\text{Ge}_x)_2$ single crystals, *Phys. Rev. Mater.* **7**, 064405 (2023).
- [26] B. Wolf, F. Spathelf, J. Zimmermann, T. Lundbeck, M. Peters, K. Kliemt, C. Krellner, and M. Lang, From magnetic order to valence-change crossover in $\text{EuPd}_2(\text{Si}_{1-x}\text{Ge}_x)_2$ using He-gas pressure, *SciPost Phys. Proc.* **11**, 022 (2023).
- [27] C. U. Segre, M. Croft, J. A. Hodges, V. Murgai, L. C. Gupta, and R. D. Parks, Valence Instability in $\text{Eu}(\text{Pd}_{1-x}\text{Au}_x)_2\text{Si}_2$: The Global Phase Diagram, *Phys. Rev. Lett.* **49**, 1947 (1982).
- [28] M. Ye, M. J. G. von Westarp, S. M. Souliou, M. Peters, R. Möller, K. Kliemt, M. Merz, R. Heid, C. Krellner, and M. L. Tacon, Strong electron-phonon coupling and enhanced phonon Grüneisen parameters in valence-fluctuating metal EuPd_2Si_2 , *Phys. Rev. B* **107**, 195111 (2023).
- [29] B. Wolf, D. A. S. Kaib, A. Razpopov, S. Biswas, K. Riedl, S. M. Winter, R. Valentí, Y. Saito, S. Hartmann, E. Vinokurova, T. Doert, A. Isaeva, G. Bastien, A. U. B. Wolter, B. Büchner, and M. Lang, Combined experimental and theoretical study of hydrostatic (He-gas) pressure effects in $\alpha\text{-RuCl}_3$, *Phys. Rev. B* **106**, 134432 (2022).
- [30] S. N. Y. Takikawa and S. Ebisu, Van Vleck paramagnetism of the trivalent Eu ions, *J. Phys. Chem. Solids* **71**, 1592 (2010).
- [31] H. Wada, H. Gomi, A. Mitsuda, and M. Shiga, Specific heat anomaly due to valence transition in $\text{Eu}(\text{Pd}_{1-x}\text{Pt}_x)_2\text{Si}_2$, *Solid State Commun.* **117**, 703 (2001).
- [32] Note that the susceptibility data of $x = 0.058$ (crystal 3) for $p = 0.43$ GPa and $p = 0.47$ GPa were omitted in the inset of Fig. 3 for clarity.
- [33] Y.-J. Song, S. Schulz, K. Kliemt, C. Krellner, and R. Valentí, Microscopic origin of the valence transition in tetragonal EuPd_2Si_2 , *Phys. Rev. B* **107**, 075149 (2023).
- [34] H. Wada, M. F. Hundley, R. Movshovich, and J. D. Thompson, Pressure effect on the valence transition of $\text{EuNi}_2(\text{Si}_{1-x}\text{Ge}_x)_2$, *Phys. Rev. B* **59**, 1141 (1999).
- [35] B. G. Schmiester, B. Perscheid, G. Kaindl, and J. Zukrowsky, Effects of pressure and temperature on the mean valence of EuPd_2Si_2 , in *Valence Instabilities*, edited by P. Wachter and H. Boppert (Elsevier, Amsterdam, Netherlands, 1981), p. 219.
- [36] V. K. Anand and D. C. Johnston, Antiferromagnetism in EuCu_2As_2 and $\text{EuCu}_{1.82}\text{Sb}_2$ single crystals, *Phys. Rev. B* **91**, 184403 (2015).
- [37] S. Watanabe and K. Miyake, Roles of critical valence fluctuations in Ce- and Yb-based heavy fermion metals, *J. Phys.: Condens. Matter* **23**, 094217 (2011).
- [38] R. S. Manna, B. Wolf, M. de Souza, and M. Lang, High-resolution thermal expansion measurements under helium-gas pressure, *Rev. Sci. Instrum.* **83**, 085111 (2012).
- [39] Y. Agarmani, S. Hartmann, J. Zimmermann, E. Gati, C. Delleske, U. Tutsch, B. Wolf, and M. Lang, Advanced technique for measuring relative length changes under control of temperature and helium-gas pressure, *Rev. Sci. Instrum.* **93**, 113902 (2022).
- [40] M. E. Fisher, Relation between the specific heat and susceptibility of an antiferromagnet, *Philos. Mag.* **7**, 1731 (1962).
- [41] B. C. Sales and D. K. Wohlleben, Susceptibility of Interconfiguration-Fluctuation Compounds, *Phys. Rev. Lett.* **35**, 1240 (1975).